

Shear wave anisotropy from cross-correlation of seismic noise in the Parkfield pilot hole

Michael A. Lewis* and Peter Gerstoft

Scripps Institution of Oceanography, La Jolla, CA 92093, USA. E-mail: m5lewis@ucsd.edu

Accepted 2011 October 31. Received 2011 October 30; in original form 2011 August 28

SUMMARY

We use cross-correlation of seismic noise recorded at stations in the San Andreas Fault Observatory at Depth (SAFOD) pilot hole to extract P and S waves and measure S -wave anisotropy on the horizontal components. The data are recorded at seven three-component stations at depths from 1857 to 2097 m in the pilot hole. In late September and early 2004 October drilling noise underneath the stations generated propagating waves, which were absent in the rest of October. Estimates of the P - and S -wave velocities from the cross-correlations, on the vertical and horizontal components, respectively, are consistent with velocity measurements taken directly in the borehole. We observe polarization of the S wave, with a fast polarization direction of 120° – 130° that is 4 per cent faster than the slow direction. Cross-correlation of the seismic noise can accurately determine S -wave anisotropy.

Key words: Interferometry; Body waves; Seismic anisotropy.

1 INTRODUCTION

The majority of noise cross-correlation studies to date have used regional scale networks of stations and obtained the Rayleigh wave portion of the Green's function (Sabra *et al.* 2005; Shapiro *et al.* 2005). Tomography conducted upon the extracted surface waves agrees well with the results derived from more traditional event-based methods. Regional scale crustal anisotropy have been determined from seismic interferometry of surface wave noise (Duret *et al.* 2010; Moschetti *et al.* 2010; Yao *et al.* 2010; Lin *et al.* 2011). Observations of body waves from seismic noise have been less common (e.g. Roux *et al.* 2005; Draganov *et al.* 2007; Gerstoft *et al.* 2008; Zhang *et al.* 2010; Ruigrok *et al.* 2011). Miyazawa *et al.* (2008) extracted the P and S waves from noise cross-correlation on a vertical array in a 400 m deep borehole and measured the polarization of downward propagating S waves. Their results suggest that when compatible noise sources and station arrangements exist, high-resolution P - and S -wave velocities and S -wave anisotropy can be extracted.

In the crust, the presence of anisotropy is generally attributed to one of two causes. The first is response of cracks to the *in situ* stress field leading to preferential closure of the fractures (Crampin 1987; Boness & Zoback 2004). This results in a fast shear wave direction parallel to the maximum compressive stress. The second cause is alignment of some structural features, such as fractures preferentially parallel to a fault (Liu *et al.* 2008); in this case the orientation of the fast shear wave depends on the orientation of the structural

feature. S -wave anisotropy studies of the crust around faults have found fast directions nearly parallel to the fault orientation (Peng & Ben-Zion 2004; Mizuno *et al.* 2005), including the San Andreas Fault (Liu *et al.* 2008). The crustal anisotropy around Parkfield has been attributed to both the *in situ* stress field and structural fabric (fault-aligned cracks) depending on the station location. In contrast to these earthquake-based studies where the measured anisotropy is distributed somewhere between the earthquake and receiver, when using noise cross-correlation estimates any observed anisotropy will be between the station pair.

2 SETTING AND DATA

The pilot and main boreholes of the San Andreas Fault Observatory at Depth (SAFOD) project are located near the town of Parkfield in central California. The area is dominated by the northwest–southeast trending San Andreas Fault system (Figs 1a and b). Studies have characterized the velocity (e.g. Thurber *et al.* 2006) and anisotropy (Liu *et al.* 2008) structure of the region. Properties of the pilot hole have been directly measured using downhole-logging instruments, including P - and S -wave velocities. Vasconcelos *et al.* (2008) demonstrated that drilling noise from the main hole was recorded in the pilot hole and used it to image the structure of the San Andreas Fault. The pilot hole was drilled in 2002 and 32 three-component GS-20DM geophone sensors were installed to make triggered recordings of earthquakes. From 2004 September 30 continuous data are available at seven stations at depths between 1857 and 2097 m with sampling rate 1 kHz. The bottom of the main hole was then 1 km to the NE at an angle of 120° to the stations in the pilot hole. Propagating P and S waves were observed coinciding with drilling activity in the main hole. The drilling noise primarily

*Now at: Earthworks Environment & Resources Ltd., Salisbury, SP2 7NU, UK.

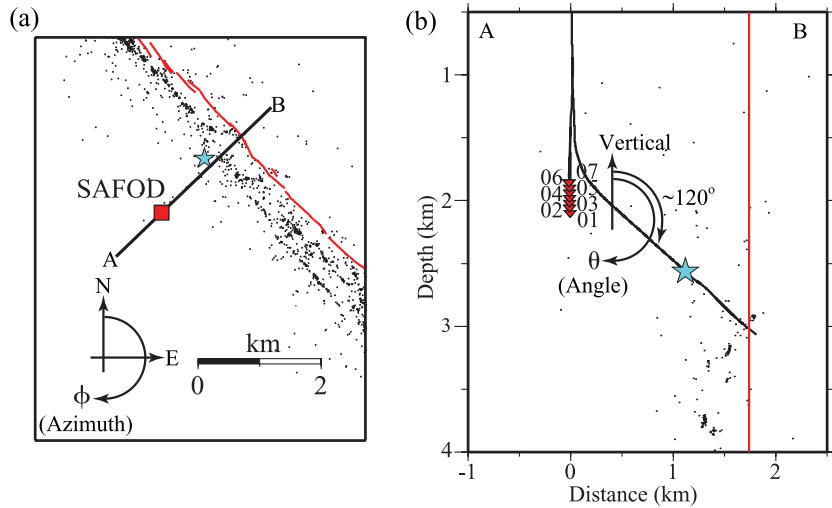


Figure 1. (a) Parkfield area showing the SAFOD site (red square), San Andreas fault (red lines), seismicity (black dots) and drilling location (blue star). (b) Cross-section along A–B in (a) showing the trajectory of the main and pilot holes (black lines) and stations used (red triangles).

occurs on October 2–3, thus all analysis is focused on these two days.

3 NOISE CORRELATION AT A VERTICAL ARRAY

Theoretical and observational studies have shown that cross-correlation of the noise recorded at two points can recover the Green’s function between those two points (Derode *et al.* 2003; Wapenaar 2004; Nakahara 2006; also see reviews Gouédard *et al.* 2008; Wapenaar *et al.* 2010). When the noise sources are spatially homogeneous, there is significant scattering or the noise sources are in line with the axis between the stations pair, the cross-correlation is expected to correspond to the Green’s function of the medium.

The stations used here are along the same axis and the noise source is at a know location. Thus the angles between the station pairs and the source are constant. Another advantage is that the array geometry works towards the recovery of the Green’s function even though the noise source is in a fixed off axis location (Harmon *et al.* 2008, 2010; Froment *et al.* 2010). In the far field for a 2-D propagating wave with angular source distribution $\rho_s(\theta)$ the cross-correlation between the signal at two stations is (Tsai 2009)

$$\rho(\Delta t) = \rho_s(\theta(\Delta t)) \cdot \frac{v/\Delta x}{\sqrt{1 - (v\Delta t/\Delta x)^2}} = \rho_s(\theta) \cdot \frac{v/\Delta x}{|\sin \theta|}, \quad (1)$$

where v is velocity, Δx station separation and θ vertical angle of source relative to the array. For an axisymmetric 3-D case $\rho = \rho_s(\theta)$. The traveltme Δt relates to angle as:

$$\Delta t = \frac{\Delta x \cos \theta}{v}. \quad (2)$$

The second part of eq. (1) shows that energy propagating close to the station axis provides a stronger contribution to the approximate Green’s function recovered from the cross-correlation (Fig. 2). Where traveltme corresponds to angles by eq. (2) when a source is located at larger Δt , closer to the station axis (here vertically, 0° or 180°), its contribution to the extracted Green’s function power is much larger than sources incident from intermediate angles (Fig. 2). Thus, for a vertical array of stations vertically propagating energy is emphasized, that is, P waves on the vertical component and S waves on the horizontal components.

The dashed lines in Fig. 2 correspond to the traveltme between the station pair of energy arriving directly from the drilling location for each of the station separations. These direct arrivals occur at traveltmes that have a low contribution to the resulting

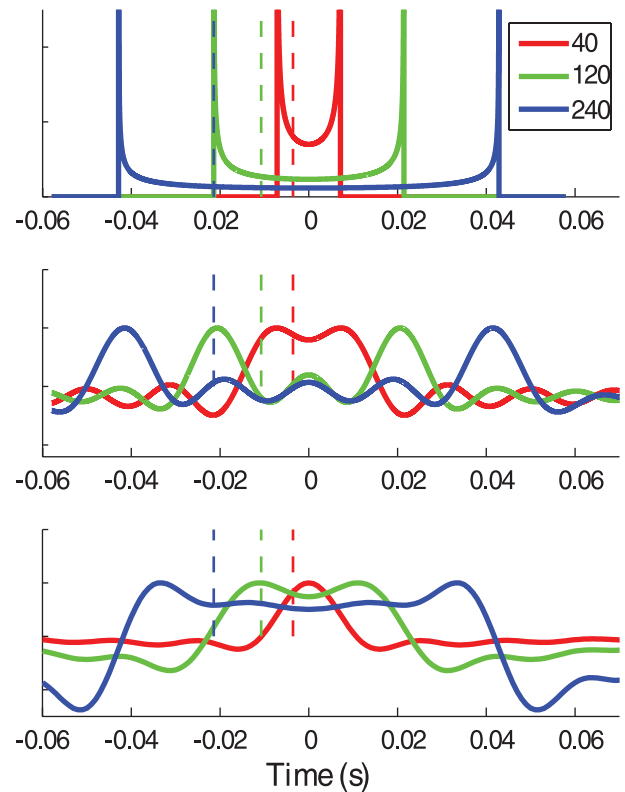


Figure 2. Density function versus traveltme delay for three station separations, 2-D (top), finite bandwidth 2-D (middle) and finite bandwidth 3-D case (bottom) for a velocity of 3.3 km s^{-1} and 5–50 Hz bandwidth. The colour represents the three station separations, 40 (red), 120 (green) and 240 m (blue). The dashed lines correspond to the arrival time directly from the angle to the drilling location. The vertical axis is normalized contribution of the noise to the recovered signal from the different traveltmes between the station pair. For assumed velocity the traveltme relates to the angle between the station pair axis and the source (eq. 2).

cross-correlation, whereas a much lower amplitude but vertically propagating signal resulting from scattering and refractions, has a much stronger contribution to the recovered Green's function. This enables us to recover the actual velocity between the station pair with minimal effect from an off axis source. If the signals used are frequency limited or in 3-D then this smears out the sharpness of the peaks, particularly when the station separation is low (middle and bottom panel of Fig. 2), however the amplification of the contribution to the Green's function from vertical incident energy still remains and given that the source and the receiver all lie in a propagation plane 2-D wave propagation seems most correct.

As a result of the array geometry energy propagating directly from the drilling location contributes less to the Green's function power. The vertically aligned fracture near the fault will preferentially scatter a small amount of the energy vertically upwards, parallel to the fractures (Schultz & Toksoz 1995; Willis *et al.* 2006), which because of the array geometry will have a stronger contribution allowing for extracting the traveltime between station pairs.

4 RESULTS

We use a discrete noise source from a well-defined direction, the drilling in the SAFOD main borehole, to estimate the P - and S -velocities between stations in the pilot borehole using seismic interferometry. Noise cross-correlations were calculated between each station pair using the data from October 2 to 3. The seismograms are 5–50 Hz bandpass filtered and amplitudes were truncated if exceeding 0.5 times the minimum of the daily SD s. The truncated waveforms were then normalized in the frequency domain to homogenize the signals. This pre-processed data was then split into 15-s segments that were cross-correlated with all stations and itself. These are then stacked over time (Fig. 3). This results in seven noise

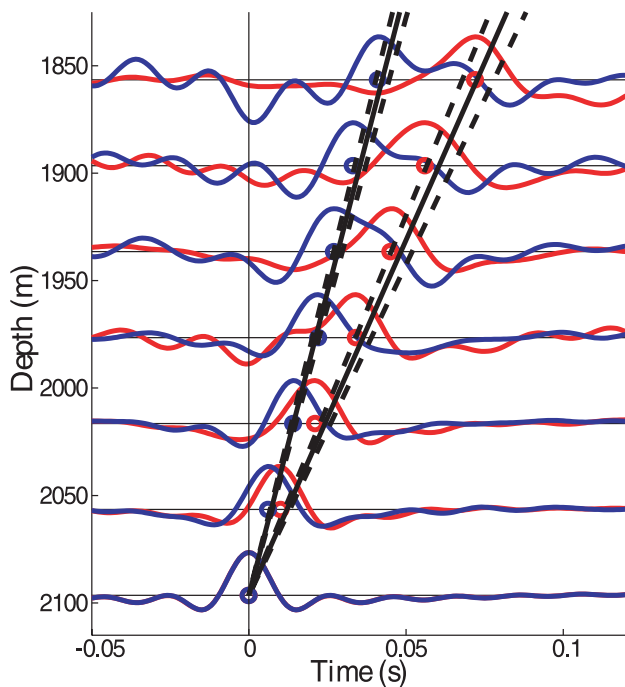


Figure 3. Normalized cross-correlations between the bottom and other stations for vertical component (blue) and N-S component (red) from October 2 to 3. Measured traveltimes (circles), the mean P - and S -wave velocity directly measured in the borehole (solid black lines) and ± 1 SD (dashed lines) are shown.

cross-correlation functions for each station. Upward propagating P and S waves are seen upon the cross-correlations from the noise on days before October 3; no such signal is seen in the data after this date when drilling was suspended for the winter. For the S -wave anisotropy analysis the procedure is repeated on the horizontal components rotated between 0° and 180° . To improve the traveltime estimates, the data were up-sampled by a factor of 10 giving a 10 kHz sampling frequency. On the horizontal components cross-correlations, S -wave velocity variations are seen in a pattern consistent with azimuthal anisotropy.

4.1 P - and S -wave velocities

The vertical and horizontal components cross-correlations, with the deepest station as reference, show upward propagating waves (Fig. 3). The autocorrelation of P and S waves (bottom trace, Fig. 3) are identical as the frequency normalization makes them identical to a sinc function with bandwidth $50-5 = 45$ Hz. The arrival times are later on the N-S component than the vertical, consistent with P - and S -wave signals.

A linear least-square fit to the arrival times (circles, Fig. 3) at each station, gives a P -velocity of 5.87 km s^{-1} and S -velocity of 3.80 km s^{-1} . These are consistent with the P - and S -wave velocities measured directly from borehole logging (5.65 and 3.31 km s^{-1}), averaged over the depth range of the stations (black lines, Fig. 3). The off-axis source is not observed in the measured velocities as it is mitigated by stronger contribution from along-axis energy (see eq. 1). The P and S waves are clearly distinct (Fig. 3) and the processing de-emphasized horizontal P waves. Further, if any P -wave energy in the horizontal components affected the measurements then a fast direction perpendicular to the fault (towards the source) would be observed.

4.2 S -wave anisotropy

Cross-correlations of the horizontal components at different azimuths reveals traveltime variations, suggesting that the S -wave velocity depends on S -wave polarization. The horizontal components at each station are rotated in 5° increments and cross-correlated with all stations, producing seven cross-correlations for each reference station at each 5° azimuth increment. For each reference station and azimuth a velocity is determined by a least-squared fit to the peak of the cross-correlations (red circles in Fig. 3). Subtracting the average velocity across azimuths gives the velocity variation with azimuth for each reference station (Fig. 4).

The velocities show a sharp minimum around $30^\circ-40^\circ$ and a broader maximum at 120° (Fig. 4) with a relative difference between fast and slow direction of 4 per cent. Using the errors in the velocity measurements, we estimate the expected deviations from a smoothly varying function averaged similar to the real data, the observed data points are within the errors (grey lines Fig. 4f). The results using stations 04 and 05 as reference stations were discarded. As these stations are in the array centre, the maximum propagation distance between station pairs is halved compared to a reference station at either end of the array. The signal-to-noise ratio with station 04 as reference is the lowest. Fig. 2 shows that the contribution of energy from along-axis directions decreases with station spacing, thus extracted traveltime is more uncertain with a centre reference station. Further, shorter propagation distance gives larger relative traveltime errors. The longer propagation distances are important for obtaining accurate velocity variations.

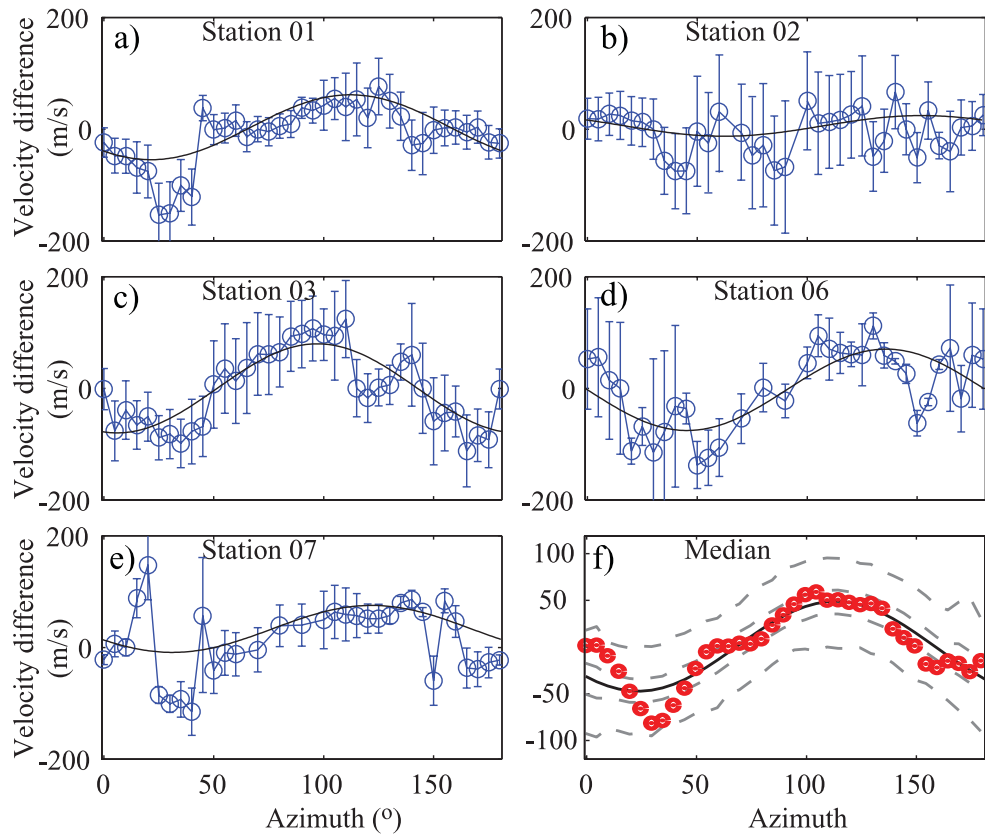


Figure 4. (a–e) The deviation of the velocity from the median versus azimuth for the horizontal components rotated through angles, the error bars are the *SE* of the least squares. Each panel represents velocities from the traveltimes obtained using a different reference stations. The best-fitting curves of the form $A + B\cos(2\phi) + C\sin(2\phi)$ are shown as solid line. (f) Median velocity from all sets of cross-correlations smoothed with a moving average (red circles). Grey dashed lines indicate the 50 and 95 per cent error interval.

The error bars in Fig. 4 are the standard error of the velocity (slope) from the least-square fit to the traveltimes at each azimuth (Gonick & Smith 1993). Averaging the errors shown in Figs 4(a)–(e) across all station pairs gives an average error in velocity of 0.9 per cent. As traveltimes are taken at the peak in amplitude, the variations in the traveltimes likely originate from the inability of the cross-correlation to accurately resolve the peak. The average direction of the maximum velocity in Figs 4(a)–(f) is 125° , excluding the points at 20° in Fig. 4(e) with a 12° *SD*. The fast direction (120° – 130°) is near to the orientation of the San Andreas Fault (132°) and as such the anisotropy is likely the result of alignment of damage and cracks with the fault, consistent in orientation and magnitude with previous results using traditional event-based techniques (Liu *et al.* 2008).

5 CONCLUSION

Noise cross-correlations from seven stations in the SAFOD pilot hole at Parkfield show upward propagating *P* and *S* waves excited by drill noise from the SAFOD main hole. The *S* waves on the horizontal components show variations in velocity with azimuth, albeit with some deviation depending on reference station. When averaged there is a clear fast *S* wave direction of 120° – 130° with 4 per cent velocity variation. The average variations with azimuth are consistent with azimuthal anisotropy from alignment of cracks parallel with the Fault. Our 120° – 130° fast direction is closer to the 132° orientation of the San Andreas Fault than the 110° reported by

Liu *et al.* (2008). This could be due to our data being immediately after the *M* 6.0 2004 Parkfield earthquake that enhanced the fault zone fabric (Brenguier *et al.* 2008; Peng & Ben-Zion 2005). The location of the noise source, at an angle to the array, is not affecting the traveltimes because the geometry causes vertical incident energy scattered towards vertical propagation has a stronger contribution to the recovered Green's function.

An off-axis source should be strongly reducing in the processing, but an off-axis source will not affect the determined fast and slow directions. Anisotropy from randomly distributed cracks with a single preferred orientation produces hexagonal anisotropy where the velocity of the body waves in the symmetry plane is $A + B\cos(2\phi) + C\sin(2\phi)$, where *A*, *B* and *C* are elastic constants and ϕ the fast direction, thus the velocity variations are independent of the incident angle. Noise cross-correlation can reveal fine scale details of the both the velocity structure and anisotropic fabric when noise sources and appropriate station configurations exist.

ACKNOWLEDGMENTS

This work was supported by U.S. Air Force Research Laboratory (FA8718–07–C–0005) and Minerals Management Service via the Gulf of Mexico Hydrates Research Consortium. Seismic data obtained from IRIS. Drilling trajectory and borehole-logging data on the SAFOD project were obtained from <http://www.icdp-online.org/>.

REFERENCES

- Boness, N. & Zoback, M., 2004. Stress-induced seismic velocity anisotropy and physical properties in the SAFOD pilot Hole in Parkfield, CA, *Geophys. Res. Lett.*, **31**, L15–L17.
- Brenguier, F., Campillo, M., Hadziioannou, C., Shapiro, N.M., Nadeau, R.M. & Larose, E., 2008. Postseismic relaxation along the San Andreas fault at Parkfield from continuous seismological observations, *Science*, **321**, 1478–1481.
- Crampin, S., 1987. The geological and industrial implications implication of extensive dilatancy anisotropy, *Nature*, **328**, 491–496.
- Derode, A., Larose, E., M. Campillo & M. Fink, 2003. How to estimate the Green's function of a heterogeneous medium between two passive sensors: application to acoustic waves, *Appl. Phys. Lett.*, **83**, 3054–3026.
- Draganov, D., Wapenaar, K., Mulder, W., Singer, J. & A. Verdel, 2007. Retrieval of reflections from seismic background 'noise' measurements, *Geophys. Res. Lett.*, **34**, L04305, doi:10.1029/2006GL028735.
- Duret, F., Shapiro, N.M., Cao, Z., Levin, V., Molnar, P. & Roecker, S., 2010. Surface wave dispersion across Tibet: direct evidence for crustal radial anisotropy in the crust, *Geophys. Res. Lett.*, **37**, doi:10.1029/2010GL043811.
- Froment, B., Campillo, M., Roux, P., Gouédard, P., Verdel, A. & Weaver, R.L., 2010. Estimation of the effect of non-isotropically distributed energy on the apparent arrival time in correlations, *Geophysics*, **75**, SA85–SA92, doi:10.1190/1.3483102.
- Gerstoft, P., Shearer, P.M., Harmon, N. & Zhang, J., 2008. Global P, PP, and PKP wave microseisms observed from distant storms, *Geophys. Res. Lett.*, **35**, L23307, doi:10.1029/2008GL036111.
- Gonick, L. & Smith, W., 1993. *The Cartoon Guide to Statistics*, pp. 202–204, Harper Perennial, New York, NY.
- Gouédard, P. *et al.*, 2008. Cross-correlation of random fields: mathematical approach and applications. *Geophys. Prospect.*, **56**, 375–393. doi:10.1111/j.1365-2478.2007.00684.x.
- Harmon, N., Gerstoft, P., Rychert, C.A., Abers, G.A., Salas de la Cruz, M. & Fischer, K.M., 2008. Phase velocities from seismic noise using beam-forming and cross correlation in Costa Rica and Nicaragua, *Geophys. Res. Lett.*, **35**, L19303, doi:10.1029/2008GL035387.
- Harmon, N., Rychert, C. & Gerstoft, P., 2010. Distribution of noise sources for seismic interferometry, *Geophys. J. Int.*, **183**, 1470–1484, doi:10.1111/j.1365-246X.2010.04802.
- Lin, F.C., Ritzwoller, M.H., Yang, Y., Moschetti, M.P. & Fouch, M.J., 2011. Complex and variable crustal and uppermost mantle seismic anisotropy in the western United States, *Nat. Geosci.*, **4**, 55–61.
- Liu, Y., Zhang, H., Thurber, C. & Roecker, S., 2008. Shear wave anisotropy in the crust around the San Andreas fault near Parkfield: spatial and temporal analysis, *Geophys. J. Int.*, **172**, 957–970.
- Mizuno, T., Ito, H., Kuwahara, Y., Imanishi, K. & Takeda, T., 2005. Spatial variation of shear-wave splitting across an active fault and its implication for stress accumulation mechanism of inland earthquakes: the Atotsugawa fault case, *Geophys. Res. Lett.*, **32**, L20305, doi:10.1029/2005GL023875.
- Miyazawa, M., Snieder, R. & Venkateraman, A., 2008. Application of seismic interferometry to extract P- and S-waves propagation and observation of shear-wave splitting from noise data at Cold Lake, Alberta, Canada, *Geophysics*, **73**, 35–40.
- Moschetti, M.P., Ritzwoller, M. H., Lin, F. & Yang, Y., 2010. Seismic evidence for widespread western-US deep-crustal deformation caused by extension, *Nature*, **464** 885–889, doi:10.1038/nature08951.
- Nakahara, H., 2006. A systematic study of the theoretical relations between spatial correlations and Green's function in one-, two- and three-dimensional random scalar wavefields, *Geophys. J. Int.*, **167**, 1097–1105.
- Peng, Z. & Ben-Zion, Y., 2004. Systematic analysis of crustal anisotropy along the Karadere-Duzce branch of the north Anatolian fault, *Geophys. J. Int.*, **159**, 253–274, doi:10.1111/j.1365-246X.2004.02379.x.
- Peng, Z. & Ben-Zion, Y., 2005. Spatio-temporal variations of crustal anisotropy from similar events in aftershocks of the 1999 M7.4 Izmit and M7.1 Duzce, Turkey, earthquake sequences, *Geophys. J. Int.*, **160**, 1027–1043.
- Roux, P., Sabra, K.G., Gerstoft, P., Kuperman, W.A. & Fehler, M.C., 2005. P-waves from cross correlation of seismic noise, *Geophys. Res. Lett.*, **32**, L19303, doi:10.1029/2005GL023803.
- Ruigrok, E., Campman, X. & Wapenaar, K., 2011. Extraction of P-wave reflections from microseisms, *C. R. Geosci.*, **343**, 512–525, doi:10.1016/j.crte.2011.02.006.
- Sabra, K.G., Gerstoft, P., Roux, P., Kuperman, W.A. & Fehler, M.C., 2005. Surface wave tomography from microseisms in Southern California, *Geophys. Res. Lett.*, **32**, doi:10.1029/2005GL023155.
- Schultz, C.A. & Toksoz, M.N., 1995. Reflections from a randomly grooved interface: ultrasonic modelling and finite-difference calculation, *Geophys. Prospect.*, **43**, 581–594.
- Shapiro, N.M., Campillo, M., Stehly, L. & Ritzwoller, M.H., 2005. High-resolution surface-wave tomography from ambient seismic noise, *Science*, **307**, 1615–1618 doi:10.1126/science.1108339.
- Thurber, C., Zhang, H., Waldhauser, F., Hardebeck, J., Michael, A. & Eberhart-Phillips, D., 2006. Three-dimensional compressional wavespeed model, earthquake relocations, and focal mechanisms for the Parkfield, California, region. *Bull. seism. Soc. Am.*, **96**, 38–49.
- Tsai, V.C., 2009. On establishing the accuracy of noise tomography travel-time measurements in a realistic medium, *Geophys. J. Int.*, **178**, 1555–1564.
- Vasconcelos, I., Snieder, R., Sava, P., Taylor, T., Malin, P. & Chavarria, A., 2008. Drill bit noise illuminates the San Andreas Fault, *EOS, Trans. Am. geophys. Un.*, **89**(38), doi:10.1029/2008EO380001.
- Wapenaar, K., 2004. Retrieving the elastodynamic Green's function of an arbitrary inhomogeneous medium by cross correlation, *Phys. Rev. Lett.*, **93**, doi:10.1103/PhysRevLett.93.254301.
- Wapenaar, K., Draganov, D., Snieder, R., Campman, X. & Verdel, V., 2010. Tutorial on seismic interferometry: Part 1-Basic principles and applications, *Geophysics*, **75**, A195–A209, doi:10.1190/1.3457445.
- Willis M.E., Burns, D.R., Rao, R., Minsley, B., Toksoz, M.N. & Vetri, L., 2006. Spatial orientation and distribution of reservoir fractures from scattered seismic energy. *Geophysics*, **71**, O43–O51.
- Yao H., van der Hilst, R.D. & Montagner, J.-P., 2010. Heterogeneity and anisotropy of the lithosphere of SE Tibet from surface wave array analysis, *J. geophys. Res.*, **115**, B12307, doi:10.1029/2009JB007142.
- Zhang, J., Gerstoft, P. & Shearer, P.M., 2010. Resolving P-wave travel-time anomalies using seismic array observations of oceanic storms, *Earth planet. Sci. Lett.*, **292**, 419–427, doi:10.1016/j.epsl.2010.02.014.